Electrochimica Acta 258 (2017) 405–413

Contents lists available at ScienceDirect

Electrochimica Acta

journal homepage: www.elsevier.com/locate/electacta

Nano vanadium nitride incorporated onto interconnected porous carbon via the method of surface-initiated electrochemical mediated ATRP and heat-treatment approach for supercapacitors

Fen Ran [a, b, *], Zhen Wang [b], Yunlong Yang [b], Zhen Liu [c], Lingbin Kong [a, b], Long Kang [a, b]

[a] State Key Laboratory of Advanced Processing and Recycling of Non-ferrous Metals, Lanzhou University of Technology, Lanzhou, 730050, PR China
[b] School of Material Science and Engineering, Lanzhou University of Technology, Lanzhou, 730050, Gansu, PR China
[c] Department of Physics & Engineering, Frostburg State University, Frostburg, MD, 21532-2303, USA

ARTICLE INFO

Article history:
Received 9 September 2017
Received in revised form
31 October 2017
Accepted 12 November 2017
Available online 15 November 2017

Keywords:
Vanadium nitride
Asymmetric supercapacitors
Carbon materials
Negative electrode

ABSTRACT

A negative electrode material of nano vanadium nitride/interconnected porous carbon (Nano-VN/IPC) is fabricated via a novel method combining surface-initiated electrochemical mediated ATRP and heat-treatment process. The structural and composition characterization display that a low crystallinity of VN nanoparticles is obtained, which distributes uniformly in the interconnected pores of the carbon scaffold materials. The high-distribution of nano-VN particles in the interconnected pores significantly enhances the usage efficiency of the electrochemistry-active materials to ensure the high electrochemical performance of the electrode materials. The interconnected pore structure is convenient for diffusion and transfer of electrolyte ions during charging-discharging process. The Nano-VN/IPC electrodes exhibit a high specific capacitance of 284.0 F/g at 0.5 A/g in 2 M KOH aqueous electrolyte with a low resistance and good rate capability. In addition, an asymmetric supercapacitor is assembled with $Ni(OH)_2$ and Nano-VN/IPC electrodes as the positive and negative electrodes. The device presents a high specific capacitance of 122 F/g at the current density of 0.5 A/g, and when the current density increases to 5 A/g the capacitance still remains 70 F/g. Remarkably, the device delivers an ultrahigh power density of 35.6 Wh/kg at a power density of 362.5 W/kg.

1. Introduction

With growing concerns on overfossil energy and ever-increasing environmental pollution, it is necessary to develop clean and sustainable and renewable energy, such as wind energy, solar energy, water energy, and so on. As the new natural energy is cyclical, the application of energy storage devices had become an indispensable key part in new energy industry. To accommodate future societal and environmental demands, there is a strong and growing demand for developing efficient energy-storage systems for applications of portable electric devices. Supercapacitor (SC) is an emerging energy storage device with high charging and discharging efficiency, long cycle life, high power density as well as high safety [1–5]. Electrode material is the key component of SCs, largely determining the device performance. According to charging and discharging mechanism, supercapacitor is generally divided into electric double-layer capacitors (EDLCs) and pseudocapacitors [6,7].

Carbon materials with high specific surface area [8–10], such as activated carbon, graphene, and carbon nanotubes, are commonly used as double layer electrode materials. EDLCs exhibit a high power density, rapid charging/discharging performance, and excellent cycle stability, but their specific capacity remain at a low level [11]. The conductive polymers [12,13], such as polyaniline, polythiophene, and polypyrrole, provide a large pseudocapacitance, but it is easy to swell and shrink [13], and had a large internal resistance. The transitional metal oxide electrodes, such as manganese oxides [14] and nickel oxides [15], had a high specific capacity, but its conductivity is poor, seriously affecting the electrode cycle stability. Transitional metal nitrides (MxNy, M = Ti [16,17], V [18–20], and Mo [21,22]) are promising electrochemical electrode materials for SCs due to high conductivity and large specific capacitance. Among all of the reported transitional metal nitrides, vanadium

* Corresponding author. State Key Laboratory of Advanced Processing and Recycling of Non-ferrous Metals, Lanzhou University of Technology, Lanzhou, 730050, PR China.
E-mail addresses: ranfen@163.com, ranfen@lut.cn (F. Ran).

https://doi.org/10.1016/j.electacta.2017.11.076
0013-4686/

nitride (VN) has attracted particular attention due to its high conductivity and wide potential range (1.2 V). However, the electrochemical performance of VN needs to be largely enhanced, and it can be foreseen that hybrid electrode materials would attract extensive attention for the fabrication of high performance SCs. Many vanadium nitride/carbon (VN/C) hybrid electrode materials had been reported [23–25], but the distribution of the active materials on carbon surface to form a high efficient electrode system during electrochemistry process need to be improved.

Herein, we report a new method combining surface-initiated electrochemical mediated ATRP and heat-treatment process to fabricate VN/C hybrid electrode materials. The key step is the SI-eATRP for grafting the ionic polymer chains, where vanadium-based compound was adsorbed and used as precursor to synthesize VN nanoparticles by thermo-treatment. The use of interconnected porous carbon (IPC) offered a convenient scaffold for diffusion and transfer of electrolyte ions during charging-discharging process. This strategy also ensured the nano VN was uniformly doped in the porous carbon substrates, which showed high electrochemical performance like high capacitance, good rate performance electrochemical reversibility as negative electrode for SCs.

2. Experimental

2.1. Chemicals

Styrene (St), acrylamide (AM), potassium iodide (KI), triethylamine (TEA), divinylbenzene (DVB, technical grade, 80%), toluene, sorbitanmonooleate (Span-80), potassium persulfate ($K_2S_2O_4$), calcium chloride ($CaCl_2$), *N, N, N′, N′*-Tetramethylethylenediamine (TMEDA), benzyltri-*n*-butylammonium chloride (BBAC), 2-bromoisobutyryl bromide (BIBB), and ammonium vanadate (NH_4VO_3) were analytical reagents. St was distilled until colorless under reduced pressure prior to use, AM was recrystallized in acetone solution, and other reagents were directly used without further purification.

2.2. Fabrication of carbon-scaffold

In a typical procedure, the oil phase containing DVB, St (DVB/St = 1:2, *V*/*V*), toluene (5 mL, used as porogen), and Span-80 (3 g, used as surfactant) was placed in a three-neck bottle and stirred with mechanical stirrer at 55 °C for 30 min to form a homogeneous phase. Subsequently, the water phase involving DI water (85 mL), $K_2S_2O_4$ (0.2 g), and $CaCl_2$ (1.0 g) was slowly added over a period of 30 min and the reaction was lasted at 55 °C for 10 min. A creamy white high internal phase emulsion slowly formed. After all the water phase was added, the stirrer paddle was gently withdrawn and the emulsion was transferred to a glass container. The container covered with a polyethylene film to reduce evaporative losses was then clamped in a water bath at 60 °C for 48 h. After this period, the product was dried in a vacuum oven at 60 °C over 24 h. The obtained product was pre-oxidized at 320 °C for 5 h at air and carbonized under N_2 atmosphere in a tube furnace at 700 °C for 2 h to fabricate carbon-scaffold, which was named as IPC.

2.3. Chemical treatment of carbon-scaffold surface

Typically, the obtained IPC was immersed into a nitric acid solution (65 *wt.* %) at the temperature of 80 °C under refluxing process for 4 h. After oxidation, the sample was recovered and washed thoroughly with distilled water until the pH was close to 7. The resultant product was further dried at 60 °C for 24 h, and then put into a single-neck bottle that containing 30 mL of isopropyl alcohol. After that, 1.5 mL of glacial acetic acid and 15 mL of saturated isopropyl alcohol of KI were added, respectively; and the reaction was lasted at 60 °C for 5 h. Then the IPC-OH was washed by DI water and methanol for several times, and dried at 60 °C for 24 h.

2.4. Initiator-immobilization

In typical, a flask containing 0.5 g of IPC-OH, 50 mL of THF, and 2.5 mL of TEA was placed into an ice bath; after being cooled to 0 °C, the mixture solution from a combination of 2.5 mL BIBB and 25 mL THF was add dropwise to the mixture with continuous stirring. The reaction was allowed to proceed at 0 °C for 5 h and then transferred into a 30 °C water bath for 24 h. After that, the obtained surface initiator (IPC-Br) were washed with the mixture of DI water and methanol for several times and dried at 60 °C for 24 h.

2.5. SI-eATRP for polymer brush

Before SI-eATRP polymerization of monomer, Firstly, the voltammograms were recorded at room temperature with an electrochemical workstation (CHI660E, Shanghai, China) using three-electrode system, a platinum plate as the working electrode, a platinum plate counter electrode, and saturated calomel electrode (SCE) as the referenced electrode. The experimental set-up is shown in Scheme S1. Cyclic voltammetry (CV) measurement was carried out at a scan rate of 5 mV/s in 45 mL blue solution of H_2O/MeOH (2:1, V/V) containing monomer AM (2.86 g), supporting electrolyte BBAC (0.7 g), the catalyst $CuBr_2$ (0.09 g) and the ligand TMEDA (0.06 g). The reduction potentials for converting Cu^{II} to Cu^{I} can be read from CV curve. Then the nickel foam coated with IPC-Br was placed around the working electrode parallel. SI-eATRP was carried out with different initiation potential (−0.08, −0.16, −0.26 and −0.30 V) in the molecular solution. After polymerization, the polymer modified carbon materials (IPC-PAM) was immersed into ethanol for 1 days, followed by being centrifuged and dried at 60 °C for 24 h.

2.6. Adsorption experiment

The homogeneous VO_3^- solution with maximum concentration was prepared by dissolving NH_4VO_3 in distilled water at room temperature. The same mass of IPC-PAM samples prepared at different initiation potentials were added into the NH_4VO_3 solution, and stirred at room temperature for 15 h. After that, the samples were centrifuged and dried under vacuum at 60 °C for 24 h.

2.7. Preparation of nano-VN/IPC

The precursors were heated in a tube furnace equipped at 600 °C for 1.5 h under a mixed atmosphere of N_2 (40 sccm) and NH_3 (60 sccm). The heating rate was controlled at 5 °C/min. The obtained Nano-VN/IPC material synthesized at different initiation potentials of 0.08, 0.16, 0.26, and 0.30 V were named as Nano-VN/IPC-0.08V, Nano-VN/IPC-0.16V, Nano-VN/IPC-0.26V, and Nano-VN/IPC-0.30V, respectively.

2.8. Materials structural characterization

FTIR spectrum was measured with FT-IR Nexus 670 instrument. The morphology and microstructure of the fabricated materials were characterized using transmission electron microscope (TEM, JEOL, JEM-2010, Japan) and scanning electron microscope (SEM, JSM-6701F, JEOL, Japan). Energy dispersive X-ray spectroscopy (EDS), and X-ray photoelectron spectra (XPS, physical Electronics UK) were measured to analyze the surface chemical composition of

the samples. The specific surface area and pore structure of the samples was characterized by Nitrogen adsorption and desorption experiments at 77 K (Micromeritics, ASAP 2010M, USA). The specific surface area was calculated from the nitrogen adsorption isotherm using Brunauer-Emmett-Teller (BET) method and Non Local Density Functional Theory (NLDFT) model was used to analyze the pore size distribution of samples.

2.9. Electrochemical performance

The working electrode was prepared for electrochemical measurement as follows:

For the single electrodes: the fabricated active material (4.0 mg), conducting graphite (0.375 mg), acetylene black (0.375 mg), and poly-tetrafluoroethylene (0.25 mg) at the weight ratio of 80: 7.5: 7.5: 5 were mixed in an agate mortar, which was coated on the nickel foam of geometric surface area of ca. 1 cm^2 as current collector. The electrode was dried under vacuum at 60 °C for 6 h, and compressed at a pressure of 10 MPa for ca.15 s to minimize the loss of electroactive materials during the electrochemical testing process.

For the asymmetric supercapacitor: to build a supercapacitor with high operating voltage and high energy density, it was important to balance the charges stored at the positive electrode (Q_+) and the negative electrode (Q_-): the mass ratio of positive and negative electrodes were calculated by the equation: $m_+/m_- = (C_- \times \triangle V_-)/(C_+ \times \triangle V_+)$, where m was the mass of eletrode material, C was the specific capacitance of eletrode material, and $\triangle V$ was the potential drop of positive or negative electrode during the discharging process. In this study, the calculated optimal mass ratio of $Ni(OH)_2$ and Nano-VN/IPC was 1:3.6. Therefore, the active material loading is 2.0 mg and 0.55 mg, respectively. The nickel foam of geometric surface area of ca. 1 cm^2 as current collector, the other steps are consistent with the single electrode.

The performance of electrochemical properties was tested using cyclic voltammetry, galvonostatic charging-discharging and electrochemical impedance spectroscopy in an electrochemical workstation (CHI660E, Shanghai, China). The cycling stability test was performed using LAND CT2001A instrument.

Regarding the Single Electrodes Test: electrochemical measurement was conducted at room temperature in a traditional three-electrode configuration containing the working electrode, a platinum gauze counter electrode, and a saturated calomel reference electrode. The alkaline solution (2 M KOH) was used as the electrolyte for electrochemical tests. Cyclic voltammetry was recorded between −1.15 and 0 V at different scan rates from 5 to 50 mV/s. For galvonostatic charging-discharging measurement, the current density was varied from 0.5 to 5 A/g within the same potential range as cyclic voltammetry measurement. Electrochemical impedance spectroscopy was acquired with a frequency range from 10^{-2} to 10^5 Hz.

Regarding the Asymmetric Supercapacitor Test: the solid-state two electrodes asymmetric supercapacitor was assembled with $Ni(OH)_2$ and Nano-VN/IPC-0.26V electrodes acted as positive and negative electrodes, respectively, using 2M KOH aqueous as electrolyte. Cyclic voltammetry was recorded at different scan rate from 10 to 50 mV/s with a potential windows ranging from 0 to 1.45 V. For galvanostatic charging-discharging measurement, the current density was varied from 0.5 to 5 A/g within the same potential range as CV measurements. Electrochemical impedance spectroscopy spectrum was acquired with a frequency range from 10^{-2} to 10^5 Hz. The cycling test was performed using LAND CT2001A instrument at a current density of 2 A/g.

The specific capacitance of electrode can be calculated from the discharging curve at different current densities by according to following equation (1):

$$C = I \times t / (\triangle V \times m) \quad (1)$$

Where C (F/g) is the specific capacitance, I (A) is the constant discharge current, $\triangle t$ (s) is the discharge time, $\triangle V$ (V) is the voltage change during discharge (excluding the *IR* drop) and m (g) is the mass of active materials of single electrode.

Energy density of the device was calculated by according to following equation (2):

$$E = C \times \triangle V^2 / (2 \times 3.6) \quad (2)$$

Power density of the device was calculated by according to following equation (3):

$$P = E \times 3600 / (\triangle t) \quad (3)$$

Where E (Wh/kg) is the energy density of device, P (W/kg) is the power density of device, C (F/g) is the specific capacitance, $\triangle V$ (V) is the voltage change during discharging process (excluding the *IR* drop) and $\triangle t$ (h) is the discharging time.

3. Results and discussion

Fabrication strategy of nano vanadium nitride/IPC (Nano-VN/IPC) can be summarized into three steps as shown in Scheme 1. Interconnected porous carbon (IPC) was synthesized as according to our previous publication [26], and showed hierarchical porous structure interconnected each other, which was beneficial to the electrochemical process during charging and discharging process. Firstly, grafting polyacrylamide (PAM) brushes onto IPC by SI-eATRP method. Electrochemically mediated polymerization was carried out at room temperature in a traditional three-electrode configuration. A negative potential was applied to reduce Cu^{II} to Cu^{I} at the working electrode, and there was a high Cu^{I} concentration near the working electrode. The initiator-immobilized IPC was placed on the working electrode, where polymerization was conducted [27–29]. Then, the IPC-PAM samples prepared at different initiation potentials were added into a NH_4VO_3 solution, which was stirred at room temperature. After that, the samples were centrifuged and dried under vacuum. Finally, the IPC-PAM-VO_3^- was heat-treated in an NH_3 atmosphere to obtain Nano-VN/IPC composite material.

It should be noted that the eATRP was the very important process for the successfully grafting the polymer brushes. The mechanism of eATRP was that air-stable Cu^{II} deactivator was reduced to Cu^{I} activator to trigger polymerization, and electrochemical methods allowed a lower oxidation state catalyst (Cu^{I}) to be reverted back to its original higher oxidation deactivator state (Cu^{II}) by simply shifting to more positive potential values [30]. Therefore, the CV curve of the electrolyte system was tested ranging from −0.35 to 0.35 V. As shown in Fig. 1, there was a pair of obvious redox peaks, and the reduction potential was −0.05 V versus SCE. In addition, the CV curve of the electrolyte system without initiator-modified electrode on the WE was tested for reading the reduction potential for Cu^{II} to Cu^{I}. There was a pair of obvious redox peaks, and the reduction potential was −0.05 V versus SCE (the red trace in Fig. S1). After confirming the reaction system was stable, the CV curve of the electrolyte system with initiator modified electrode on the WE was tested, the shape of CV curve showed no obvious change (the black trace in Fig. S1 and Fig. 1), indicating the permeability of the initiator modified electrode was not confounding a well defined redox peak. Furthermore, the growth kinetics of polymerization reaction depend on the Cu^{II}/Cu^{I} ratio,

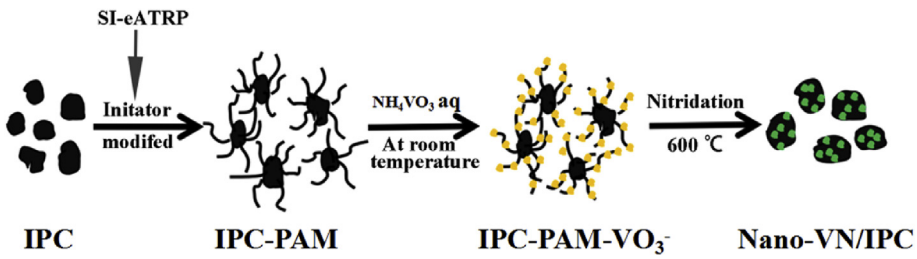

Scheme 1. Schematic illustration of the synthesis process for Nano-VN/IPC.

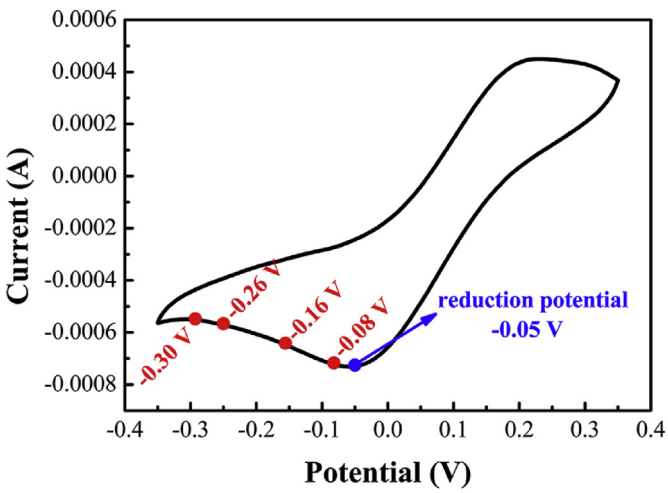

Fig. 1. Cyclic voltammogram curve of the electrolyte system at a scan rate of 5 mV/s (adjusting the applied negative potentials were highlighted with red solid point). (For interpretation of the references to colour in this figure legend, the reader is referred to the web version of this article.)

which can be adjusted by varying the applied potentials. When eATRP was carried out at positive potential or zero point no polymerization happened. The more negative potential leads to a higher Cu^{I}, and therefore the reaction occurred more rapidly but with less control [29]. Here we selected the four negative potentials from −0.35 to −0.05 V (highlighted with red solid point in Fig. 1), which will be used for the following eATRP. The reduction of Cu^{II} to Cu^{I} was an initiation step for the SI-eATRP polymerization of the PAM, so the eATRP was carried at constant applied potential. As shown in Fig. 1 with the same three-electrode system in the blue solution and as above-mentioned in Scheme S1b, there was a difference that an initiator-modified substrate was placed in counterpart position of the working electrode. Cu^{I} activator was generated at the platinum working electrode under a constant potential [28,29], and eATRP was initiated when Cu^{I} diffused to the initiator modified substrates faced to platinum working electrode and continued for 10 h at room temperature to yield polymer brushes. The surface initiator of IPC-Br and the polymer brushes grafted carbon of IPC-PAM were characterized by FTIR measurement, as shown in Fig. S2. Compared with the spectrum of IPC-Br, the band centered at 1690 cm^{-1} was the stretching vibration of C=O of -PAM block; the peak at 1566 cm^{-1} was corresponded to the bending vibration of N-H at the amide group of PAM blocks.

The morphologies and microstructures of Nano-VN/IPC composite material were examined by SEM, TEM, EDX and elemental mapping analysis as shown in Fig. 2. The microscopy image of the material exhibited obvious interconnected pore structure and there were many micrometer length scale pores of IPC (Fig. 2a). Further, from the TEM images of IPC and nano-VN/IPC as shown in Fig. S3, it was observed that there were a number of particles with nano structure (highlighted with red rings) distributed throughout the whole nano-VN/IPC surfaces of the carbon substrate (Fig. S3b), compared with that of pristine carbon of IPC. The average grain diameter was about 10–15 nm. On the other hand, the TEM image of nano-VN/IPC with high magnification has been tested and shown in Fig. 2b and c. One can find that the crystallinity of the VN was very low, while the lattice fringe can be obviously observed (0.239 nm), which is characterized to the VN material [23]. The EDS analysis shown in Fig. S3c exhibited the existences of C, O, N, V and Cu peaks, the peak of Cu was corresponding to the grid used to support the sample during the test of TEM [31]. In addition, it was no doubt that Cu ions will remain in the sample after the SI-eATRP polymerization, due to the fact that the concentration values of Cu ions was very small (ca. 8.954×10^{-3} mol/L). Therefore, the amount of copper ions contained in the sample is also very low, and the effect on electrochemical performance was almost negligible. The SAED (the inset in Fig. 2c) exhibited low crystallinity of VN nanoparticles in composite material, indicating to the presence of unreplaced oxygen atoms of the VN lattice [32], which provided more active sites for both adsorption and faradic reaction. Therefore, the lower degree of crystallinity was beneficial to electrochemical performance [33]. In addition, Fig. 2d shows the TEM elemental mapping images of composite material, and the C, O, N, and V elements were homogeneously distributed in the composite material. From these results, it can be concluded that the VN nanoparticles with a low crystallinity distributed uniformly in the surface carbon scaffold materials.

Nitrogen sorption experiment was performed to evaluate the overall porosity of the Nano-VN/IPC, as shown in Fig. 3a and 3b. The N_2 adsorption-desorption isothermal showed a typical type IV adsorption-desorption isotherm, indicative of a uniform mesopore structure [34,35], and the BET specific surface area was calculated to be 483 m^2/g. The corresponding pore size distribution represented that the obtained Nano-VN/IPC possessed mesoporous (2–6 nm), which was beneficial to the electrolyte ions to penetrate into pores of the material and improve its electrochemical capacitive properties.

The surface chemical composition of Nano-VN/IPC sample was further analyzed by XPS as shown in Fig. 4. The full XPS spectrum showed that the prepared composite material mainly composed of C, N, V, and O elements, which was consistent with the results from the EDS measurements, where O signal was attributed to the surface oxidation of VN [31,36]. The peaks at 285, 400, 535, and 520 eV in full spectra corresponded to C 1s, N 1s, O 1s and V 2p, respectively (Fig. 4a). The curve fitting of C 1s core level peak of the XPS spectrum was divided into three main peaks, including C=C (284.8 eV), C-N (286.4 eV), and C=O bonds (288.9 eV) [32,37], respectively (Fig. 4b). Due to the binding energy of the characteristic peaks of O 1s and V 2p was very close, they were usually put together for analysis. As shown in Fig. 4c, the O 1s spectrum was

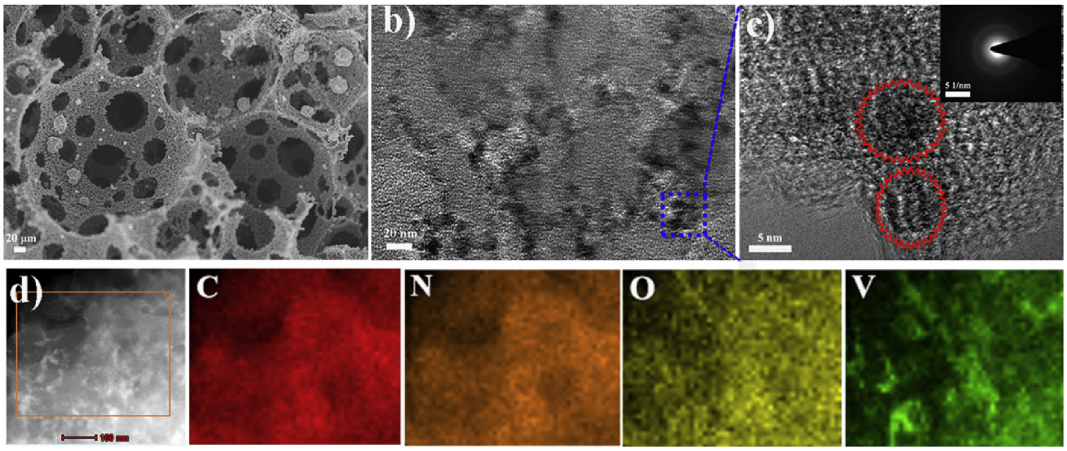

Fig. 2. a) SEM image of IPC; b and c) TEM image of Nano-VN/IPC composite material (inset is the selected-area electron diffraction pattern); and d) TEM elemental mapping images for C, N, O, and V elements.

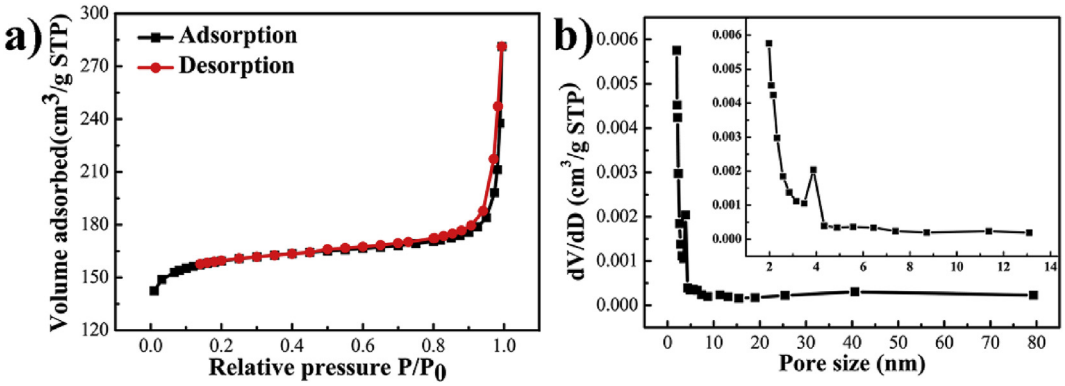

Fig. 3. a) Nitrogen adsorption and desorption isotherms, and b) pore size distribution of Nano-VN/IPC.

divided into two main peaks centered at 530.1 and 532.7 eV, respectively. Moreover, the peak at 530.1 eV indicated the existence of a complex mixture of vanadium oxides on the surface of Nano-VN/IPC, which include several vanadium oxides with different valence states of V that cannot transform to nitrides completely [38]. Another peak at 532.7 eV belonged to presence of oxygen in −OH groups at the surface of Nano-VN/IPC [39]. Bondarenka et al. [40] have conducted a useful statistical analysis of XPS data on the binding energies of V 2p spectrum, V $2p^1$ and V $2p^3$ appear to be a sum of the special lines from several valence states. The curve fitting of V $2p^3$ core level peak was divided into tow main peaks; and the peaks at 514.1 eV belonged to the main structure of VN [38,39,41], and the peaks at 517.2 eV corresponded to the V-O bond on Nano-VN/IPC [41–43]. Additionally, for the N 1s spectra, it was fitted with two peaks occurred at 397.4 and at 401.0 eV (Fig. 4d), corresponding to the characteristic of VN [44] and N-O or N-H bond [45], respectively. Through the analysis of the XPS spectra, one could be provided definite evidence that Nano-VN/IPC composed of VN and carbon, together with little amount of complex vanadium oxide on the surface. The XPS spectra of the other samples are shown in Fig. S4.

Fig. 5 depicts the electrochemical performance of Nano-VN/IPC and IPC electrodes. By comparison of the CV curves at 10 mV/s (Fig. 5a), the IPC electrode presented quasi-rectangular shape without obvious redox peaks, showing a typical electrical double layer capacitive behavior. It was found that the surrounded area of Nano-VN/IPC electrode increased profoundly with two symmetrical redox peaks, due to the presence of OH^- ions, an equilibrium reaction could occur on the nitride or oxy-nitride surface as follows: $VN_xO_y + OH^- \leftrightarrow VN_xO_y||OH^- + VN_xO_y{-}OH$, where $VN_xO_y||OH^-$ represented the electric double-layer capacitance formed by the adsorption/desorption of hydroxylions on the surface of VNand electrolyte, and $VN_xO_y{-}OH$ represented the part of pseudo-capacitance derived from the faradaic reaction that occurs on the surface of partially oxidized VN [41]. Meanwhile, the IPC electrode also provided partial electric double layer capacitance. In addition, due to the larger the specific surface area of the Nano-VN/IPC, the large contact area between the electrode and the electrolyte, and the more active sites for the electrochemical process could provide more electrical double-layer capacitance and pseudocapacitance. The GCD curves of the samples were tested at the current density of 0.5 A/g. As shown in Fig. 5b, IPC showed a closely linear and almost symmetrical triangular shape, suggesting a good electrical double layer capacitive behavior; while the GCD curve of Nano-VN/IPC electrode showed slightly shift from linear property, indicating that VN nanoparticles provided a certain pseudo-capacitance. The calculated specific capacitances of Nano-VN/IPC and IPC electrodes were 284.0 and 99.0 F/g, respectively. The rate performances of Nano-VN/IPC and IPC remained about 65% and 73% of the initial specific capacitances when the current density was increased from 0.5 to 5 A/g (Fig. 5c). It should be noted that the potential range of Nano-VN/IPC electrode was 1.15 V, higher than that of IPC. To further revealing the essence of electrochemical reaction, the electrochemical impedance spectroscopy (EIS) was

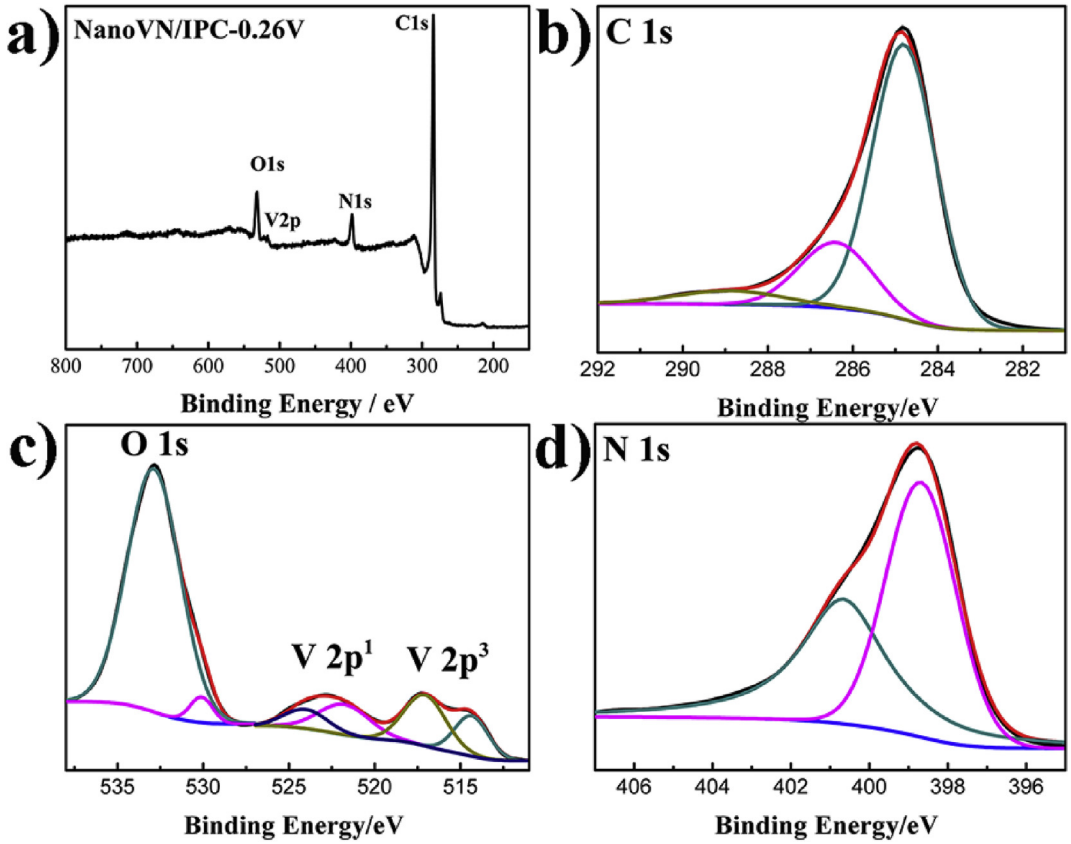

Fig. 4. XPS data: a) full spectra and b-d) other curve fittings of O1s, V2p, N1s, and C1s core level peaks for Nano-VN/IPC.

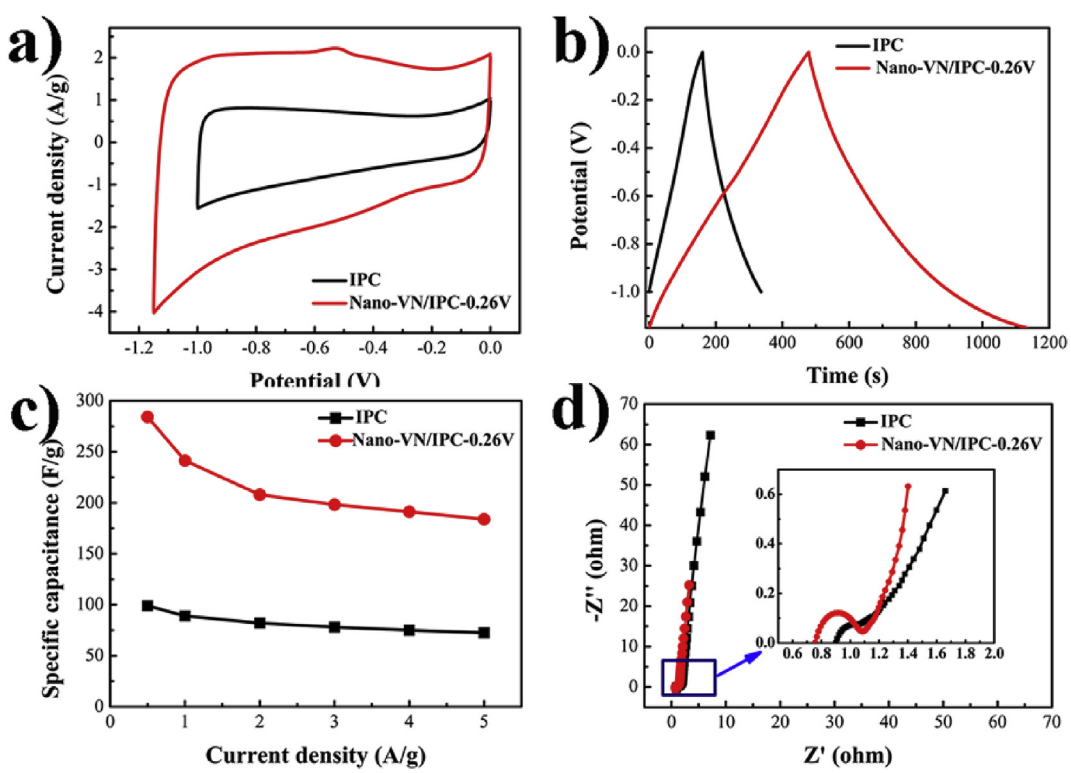

Fig. 5. Electrochemical performance for IPC and Nano-VN/IPC: a) CV curves at 10 mV/s, b) GCD curves at 0.5 A/g, c) specific capacitances at different current density, and d) Nyquist plots.

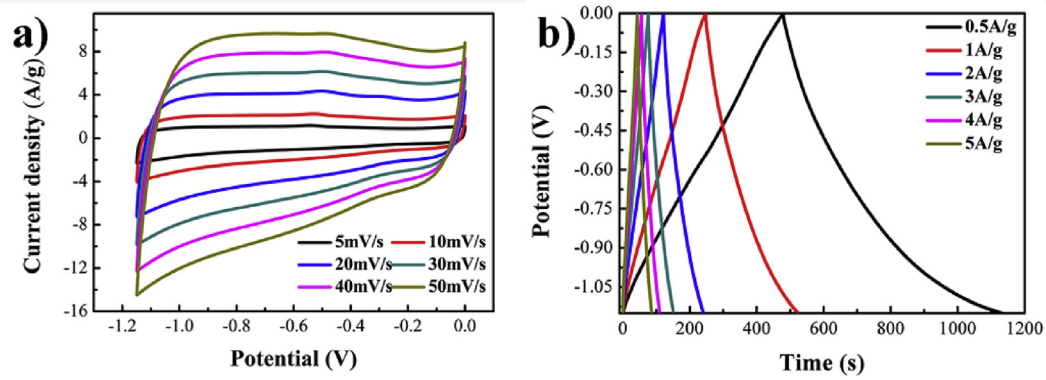

Fig. 6. a) CV curves at various scan rates; and b) GCD curves at various currents density for Nano-VN/IPC electrode.

tested, as shown in Fig. 5d. In the high frequency region, the semicircle shape represented the charge-transfer resistance (R_{ct}), R_{ct} mainly came from the electronic and ionic resistances at the interface between the electrode and the electrolyte [46]. The intercepts with the x-real axis was sintrinsic ohmic resistance (R_s), where Rs mainly came from the intrinsic resistances of electrode material, electrolyte, current collector, leads and separator, as well as the contact resistances between them [47]. In the low frequency region of the EIS was Warburg diffusion resistance (R_w), where R_w came from the resistance for ion diffusion from electrolyte into the electrode, R_w also depended on the influencing factors for R_{ct} [48,49]. Compared to IPC electrode, Nano-VN/IPC electrode displayed small R_s and R_{ct} (inset in Fig. 5d), due to the fact that VN nanoparticles homogeneously distributed throughout the carbon substrate improve electrical conductivity and wettability of the electrode materials. And it also displayed vertical slope at the low frequency region, indicating a nearly ideal capacitive behavior and low R_w at electrode/electrolyte interface.

All CV curves showed approximately aquasi-rectangular shape with a pair of redox humps observed at the potential ranging from −0.6 to −0.4 V (Fig. 6a), implying the capacitive mechanism of Nano-VN/IPC composed of both electrical double layer capacitive behavior and pseudo-capacitance behavior [23]. And the shape of CV curves at different scan rates showed no obvious change, indicating an ideal capacitive behavior of the electrode materials. In addition, the GCD curves of Nano-VN/IPC at different current densities showed linear and symmetric triangular shapes and low IR drops, indicating excellent columbic efficiency and good electrochemical reversibility during the process of charge storage (Fig. 6b). The calculated specific capacitance of the electrode material was 284 F/g at the current density of 0.5 A/g. The other samples of Nano-VN/IPCs were also prepared through synthesizing polymer brushes on IPC by using SI-eATRP under different electrochemical potential. The Nano-VN/IPCs under −0.08, −0.16, and −0.30 V were termed as Nano-VN/IPC-0.08V, Nano-VN/IPC-0.16V, and Nano-VN/IPC-0.30V. All of the CV and GCD curves for those samples are also shown in

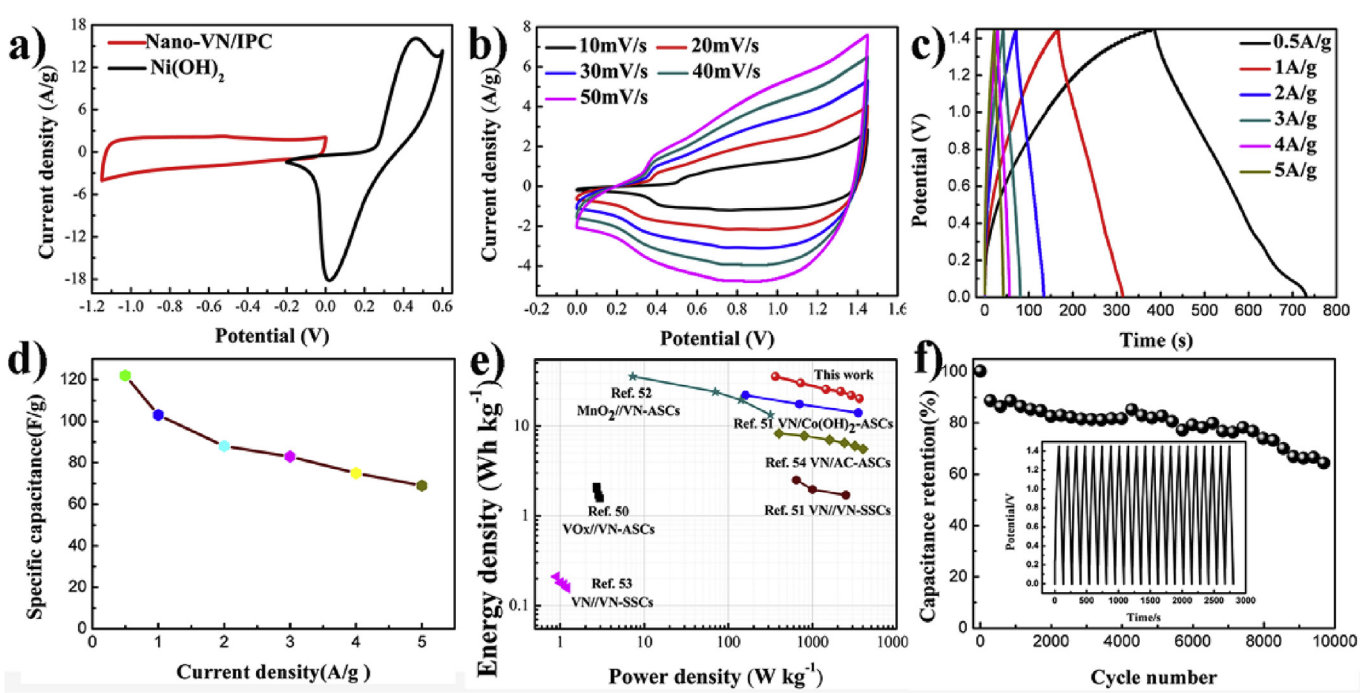

Fig. 7. a) CV curves for $Ni(OH)_2$ and Nano-VN/IPC electrodes at 10 mV/s in a three-electrode cell in 2 M KOH, respectively, and electrochemical performance of $Ni(OH)_2$||Nano-VN/IPC ASC device: b) CV curves at various scan rates; c) GCD curves at various currents density; d) The specific capacitances at different current density; e) Ragone plot; and f) cycling stability.

Fig. S5. One can see that the electrochemical performances for Nano-VN/IPC-0.08V, Nano-VN/IPC-0.16V, and Nano-VN/IPC-0.30V were as good as IPC, revealing that the potential range of from −0.30 to −0.08 V was the efficient potential windows for grafting polymer brushes and further fabricating Nano-VN/IPC electrode materials.

An asymmetric supercapacitor (ASC) was assembled with $Ni(OH)_2$ and Nano-VN/IPC electrode acted as the positive and negative electrodes, respectively. The $Ni(OH)_2$ was employed due to its potential window ranging from −0.2 to 0.6 V, matched well to that ranging from −1.15 to 0 V of Nano-VN/IPC electrode. The Nano-VN/IPC electrode and $Ni(OH)_2$ electrode were tested at a scan rate of 10 mV/s at the potential window ranging from −1.15 to 0 V, and −0.2 to 0.6 V, respectively, as shown in Fig. 7a. As such, the $Ni(OH)_2$||Nano-VN/IPC ASC was operated up to 1.45 V without obvious increase of anodic current (Fig. S6). The electrochemical performance of $Ni(OH)_2$||Nano-VN/IPC ASC device was measured in 2M KOH aqueous solution as electrolyte. CV curves of the ASC at scanning rates from 10 to 50 mV/s (Fig. 7b) exhibited a couple of little oxidation and reduction humps, which represented the pseudo-capacitive properties corresponding the redox reactions on the surface of $Ni(OH)_2$ and Nano-VN/IPC. The shape of CV curves at different scan rates showed no obvious change, indicating an ideal capacitive behavior and remarkable rate performance. The GCD curves at different current densities from 0.5 to 5 A/g showed non-linear symmetric triangular shapes and low IR drops (Fig. 7c), indicating excellent columbic efficiency and low internal series resistance. The maximum specific capacitance values calculated from GCD curve was 122 F/g at the current density of 0.5 A/g, and when the current density increased to 5 A/g the capacitance still remained 70 F/g. Fig. 7d shows the rate capability of a ASC, approximately 57.4% of initial specific capacitance was remained when the current density increased from 0.5 to 5 A/g. Energy density and power density were two important parameters for the evaluation of the device, and the Ragone plots of ASC (Fig. 7e) were calculated, which showed energy density of 35.6 Wh/kg when the power density was 362.5 W/kg. Even when the power density increased to 3625.0 W/kg, the energy density still remained 20.2 Wh/kg, which was higher than these of recently reported various VN-based device, such as VO_X||VN-ASCs [50], VN||$Co(OH)_2$-ASC [51], VN||VN-SSCs [52], VN||MnO_2-ASCs [53], and VN||AC-ASCs [54]. As shown in Fig. 7f, the ASC exhibited excellent cycling stability with 65% capacitance retention after 10000 cycles at the current density of 2 A/g.

4. Conclusions

In summary, a negative electrode of composite material Nano-VN/IPC was prepared via a method with surface-initiated electrochemical mediated ATRP and heat-treatment method, which integrates interconnected pore structure with nano VN particles uniformly doped in the porous carbon substrates. Good electrochemical behaviors, such as low resistance, high specific capacitance, and excellent cycling stability were obtained. When the applied trigger potential was −0.26V, the specific capacitance of Nano-VN/IPC had a maximum value was 284.0 F/g at the current density of 0.5 A/g in 2M KOH aqueous electrolyte. Further, the ASCs based on $Ni(OH)_2$ and Nano-VN/IPC electrodes delivered the ultrahigh power density of 35.6 Wh/kg at a power density of 362.5 W/kg, which was higher than these of recently reported various VN-based device. This work not only provided a novel method for the preparation of composite VN/C electrode materials, but also expanded to other transition-metal nitride for the application supercapacitors and other energy storage device.

Acknowledgments

This work was partly supported by the National Natural Science Foundation of China (51203071, 51363014, 51463012, and 51763014), China Postdoctoral Science Foundation (2014M552509, and 2015T81064), Natural Science Funds of the Gansu Province (2015GS05123), and the Program for Hongliu Distinguished Young Scholars in Lanzhou University of Technology (J201402).

Appendix A. Supplementary data

Supplementary data related to this article can be found at https://doi.org/10.1016/j.electacta.2017.11.076.

References

[1] J.R. Miller, P. Simon, Electrochemical capacitors for energy management, Sci. Mag. 321 (5889) (2008) 651–652.
[2] Y. Gogotsi, P. Simon, True performance metrics in electrochemical energy storage, Science 334 (6058) (2011) 917–918.
[3] P. Xiong, J. Zhu, X. Wang, Recent advances on multi-component hybrid nanostructures for electrochemical capacitors, J. Power Sources 294 (2015) 31–50.
[4] Y.T. Tan, Y. Liu, L.B. Kong, et al., Supercapacitor electrode of nano-Co3O4 decorated with gold nanoparticles via in-situ reduction method, J. Power Sources 363 (2017) 1–8.
[5] P. Simon, Y. Gogotsi, Materials for electrochemical capacitors, Nat. Mater. 7 (11) (2008) 845–854.
[6] W. Wei, X. Cui, W. Chen, et al., Manganese oxide-based materials as electrochemical supercapacitor electrodes, Chem. Soc. Rev. 40 (3) (2011) 1697–1721.
[7] Y.S. Yun, S.Y. Cho, J. Shim, et al., Microporous carbon nanoplates from regenerated silk proteins for supercapacitors, Adv. Mater. 25 (14) (2013) 1993–1998.
[8] Zhao X N, Ran F, Shen K W, et al. Facile fabrication of ultrathin hybrid membrane for highly flexible supercapacitors via in-situ phase separation of polyethersulfone[J]. J. Power Sources, 329: 104–114.
[9] S. Nardecchia, D. Carriazo, M.L. Ferrer, et al., Three dimensional macroporous architectures and aerogels built of carbon nanotubes and/or graphene: synthesis and applications, Chem. Soc. Rev. 42 (2) (2013) 794–830.
[10] E. Frackowiak, V. Khomenko, K. Jurewicz, et al., Supercapacitors based on conducting polymers/nanotubes composites, J. Power Sources 153 (2) (2006) 413–418.
[11] T. Lin, I.W. Chen, F. Liu, et al., Nitrogen-doped mesoporous carbon of extraordinary capacitance for electrochemical energy storage, Science 350 (6267) (2015) 1508.
[12] G.A. Snook, P. Kao, A.S. Best, Conducting-polymer-based supercapacitor devices and electrodes, J. Power Sources 196 (1) (2011) 1–12.
[13] T. Liu, L. Finn, M. Yu, et al., Polyaniline and polypyrrole pseudocapacitor electrodes with excellent cycling stability, Nano Lett. 14 (5) (2014) 2522–2527.
[14] Z. Fan, J. Yan, T. Wei, et al., Asymmetric supercapacitors based on graphene/MnO_2 and activated carbon nanofiber electrodes with high power and energy density, Adv. Funct. Mater. 21 (12) (2011) 2366–2375.
[15] M.M. Sk, C.Y. Yue, K. Ghosh, et al., Review on advances in porous nanostructured nickel oxides and their composite electrodes for high-performance supercapacitors, J. Power Sources 308 (2016) 121–140.
[16] D. Sun, J. Lang, X. Yan, et al., Fabrication of TiN nanorods by electrospinning and their electrochemical properties, J. Solid State Chem. 184 (5) (2011) 1333–1338.
[17] B.A. Deore, I. Yu, M.S. Freund, A switchable self-doped polyaniline: interconversion between self-doped and non-self-doped forms, J. Am. Chem. Soc. 126 (1) (2004) 52–53.
[18] R. Lucio-Porto, S. Bouhtiyya, J.F. Pierson, et al., VN thin films as electrode materials for electrochemical capacitors, Electrochim. Acta 141 (2014) 203–211.
[19] A. Morel, Y. Borjon-Piron, R.L. Porto, et al., Suitable conditions for the use of vanadium nitride as an electrode for electrochemical capacitor, J. Electrochem. Soc. 163 (6) (2016) A1077–A1082.
[20] P.J. Hanumantha, M.K. Datta, K. Kadakia, et al., Vanadium nitride supercapacitors: effect of processing parameters on electrochemical charge storage behavior, Electrochim. Acta 207 (2016) 37–47.
[21] J. Liu, K. Huang, H.L. Tang, et al., Porous and single-crystalline-like molybdenum nitride nanobelts as a non-noble electrocatalyst for alkaline fuel cells and electrode materials for supercapacitors, Int. J. Hydrogen Energy 41 (2) (2016) 996–1001.
[22] X.L. Li, X. Yan, W. Hua, et al., Synthesis and characterization of uniform nanoparticles of γ-Mo_2N for supercapacitors, Trans. Nonferr. Met. Soc. China 19 (3) (2009) 620–625.
[23] Y. Yang, L. Zhao, K. Shen, et al., Ultra-small vanadium nitride quantum dots embedded in porous carbon as high performance electrode materials for

capacitive energy storage, J. Power Sources 333 (2016) 61–71.
[24] K. Huang, K. Bi, C. Liang, et al., Novel VN/C nanocomposites as methanol-tolerant oxygen reduction electrocatalyst in alkaline electrolyte, Sci. Rep. 5 (2015) 11351.
[25] Y. Wu, F. Ran, Vanadium nitride quantum dot/nitrogen-doped microporous carbon nanofibers electrode for high-performance supercapacitors, J. Power Sources 344 (2017) 1–10.
[26] K. Shen, F. Ran, Y. Tan, et al., Toward interconnected hierarchical porous structure via chemical depositing organic nano-polyaniline on inorganic carbon scaffold for supercapacitor, Synth. Met. 199 (2015) 205–213.
[27] C. Wang, R. Feng, F. Yang, Enhancing the hydrophilic and antifouling properties of polypropylene nonwoven fabric membranes by the grafting of poly (N-vinyl-2-pyrrolidone) via the ATRP method, J. Colloid Interface Sci. 357 (2) (2011) 273–279.
[28] B. Li, B. Yu, W.T.S. Huck, et al., Electrochemically induced surface-initiated atom-transfer radical polymerization, Angew. Chem. 124 (21) (2012) 5182–5185.
[29] B. Li, B. Yu, W.T.S. Huck, et al., Electrochemically mediated atom transfer radical polymerization on nonconducting substrates: controlled brush growth through catalyst diffusion, J. Am. Chem. Soc. 135 (5) (2013) 1708–1710.
[30] A.J.D. Magenau, N.C. Strandwitz, A. Gennaro, et al., Electrochemically mediated atom transfer radical polymerization, Science 332 (6025) (2011) 81–84.
[31] X. Xiao, X. Peng, H. Jin, et al., Freestanding mesoporous VN/CNT hybrid electrodes for flexible all-solid-state supercapacitors, Adv. Mater. 25 (36) (2013) 5091–5097.
[32] E.F. De Souza, C.A. Chagas, T.C. Ramalho, et al., A combined experimental and theoretical study on the formation of crystalline vanadium nitride (VN) in low temperature through a fully solid-state synthesis route, J. Phys. Chem. C 117 (48) (2013) 25659–25668.
[33] Y. Xu, J. Wang, L. Shen, et al., One-dimensional vanadium nitride nanofibers fabricated by electrospinning for supercapacitors, Electrochim. Acta 173 (2015) 680–686.
[34] Y. Meng, D. Gu, F. Zhang, et al., A family of highly ordered mesoporous polymer resin and carbon structures from organic-organic self-assembly, Chem. Mater. 18 (18) (2006) 4447–4464.
[35] H. Fan, F. Ran, X. Zhang, et al., Easy fabrication and high electrochemical capacitive performance of hierarchical porous carbon by a method combining liquid-liquid phase separation and pyrolysis process, Electrochim. Acta 138 (2014) 367–375.
[36] Y. Liu, L. Liu, L. Kong, et al., Supercapacitor electrode based on nano-vanadium nitride incorporated on porous carbon nanospheres derived from ionic amphiphilic block copolymers & vanadium-contained ion assembly systems, Electrochim. Acta 211 (2016) 469–477.
[37] A.M. Glushenkov, D. Hulicova-Jurcakova, D. Llewellyn, et al., Structure and capacitive properties of porous nanocrystalline VN prepared by temperature-programmed ammonia reduction of V_2O_5, Chem. Mater. 22 (3) (2009) 914–921.
[38] B. Gao, X. Li, X. Guo, et al., Nitrogen-doped carbon encapsulated mesoporous vanadium nitride nanowires as self-supported electrodes for flexible all-solid-state supercapacitors, Adv. Mater. Interfaces 2 (13) (2015).
[39] X. Zhou, C. Shang, L. Gu, et al., Mesoporous coaxial titanium nitride-vanadium nitride fibers of core-shell structures for high-performance supercapacitors, ACS Appl. Mater. Interfaces 3 (8) (2011) 3058–3063.
[40] V. Bondarenka, Valence of vanadium in hydrated compounds, Lith. J. Phys. Tech. Sci. 47 (2007) 333–342.
[41] D. Choi, G.E. Blomgren, P.N. Kumta, Fast and reversible surface redox reaction in nanocrystalline vanadium nitride supercapacitors, Adv. Mater. 18 (9) (2006) 1178–1182.
[42] H.M. Lee, G.H. Jeong, S.W. Kim, et al., Low-temperature direct synthesis of mesoporous vanadium nitrides for electrochemical capacitors, Appl. Surf. Sci. 400 (2017) 194–199.
[43] X. Liang, C.Y. Kwok, F. Lodi-Marzano, et al., Tuning transition metal oxide-sulfur interactions for long life lithium sulfur batteries: the"Goldilocks"principle, Adv. Energy Mater. 6 (6) (2016).
[44] Y.U.M. Shulga, V.N. Troitskii, M.I. Aivazov, et al., X-ray photo-electron spectra of the mononitrides of Sc, Ti, V and Cr, Zh. Neorg. Khim 21 (10) (1976) 2621–2624.
[45] F. Cheng, C. He, S. Dong, et al., Preparation of nanocrystalline VN by the melamine reduction of V_2O_5 xerogel and its supercapacitive behavior, Mater. Chem. Phys. 131 (1–2) (2011) 268–273.
[46] J. Luo, H.D. Jang, J. Huang, Effect of sheet morphology on the scalability of graphene-based ultracapacitors, ACS Nano 7 (2) (2013) 1464–1471.
[47] J. Zhao, Y. Jiang, H. Fan, et al., Porous 3D few-layer graphene-like carbon for ultrahigh-power supercapacitors with well-defined structure-performance relationship, Adv. Mater. 29 (11) (2017) 1604569.
[48] J. Zhao, H. Lai, Z. Lyu, et al., Hydrophilic hierarchical nitrogen-doped carbon nanocages for ultrahigh supercapacitive performance, Adv. Mater. 27 (23) (2015) 3541–3545.
[49] Z. Bo, W. Zhu, W. Ma, et al., Vertically oriented graphene bridging active-layer/current-collector interface for ultrahigh rate supercapacitors, Adv. Mater. 25 (40) (2013) 5799–5806.
[50] X. Lu, M. Yu, T. Zhai, et al., High energy density asymmetric quasi-solid-state supercapacitor based on porous vanadium nitride nanowire anode, Nano Lett. 13 (6) (2013) 2628–2633.
[51] R. Wang, X. Yan, J. Lang, et al., A hybrid supercapacitor based on flower-like $Co(OH)_2$ and urchin-like VN electrode materials, J. Mater. Chem. A 2 (32) (2014) 12724–12732.
[52] Y. Su, I. Zhitomirsky, Hybrid MnO_2/carbon nanotube-VN/carbon nanotube supercapacitors, J. Power Sources 267 (2014) 235–242.
[53] Y. Yang, K. Shen, Y. Liu, et al., Novel Hybrid nanoparticles of vanadium nitride/porous carbon as an anode material for symmetrical supercapacitor, Nano-Micro Lett. 9 (1) (2017) 6.
[54] Y. Wang, M. Jiang, Y. Yang, et al., Hybrid electrode material of vanadium nitride and carbon fiber with cigarette butt/metal ions wastes as the precursor for supercapacitors, Electrochim. Acta 222 (2016) 1914–1921.